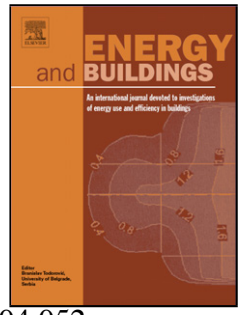

Title: Energy and exergy analysis of different Trombe walls

Author: Shuangping Duan Chengjun Jing Zhiqiang Zhao

PII: S0378-7788(16)30317-6
DOI: http://dx.doi.org/doi:10.1016/j.enbuild.2016.04.052
Reference: ENB 6603

To appear in: *ENB*

Received date: 22-4-2015
Revised date: 9-4-2016
Accepted date: 22-4-2016

Please cite this article as: Shuangping Duan, Chengjun Jing, Zhiqiang Zhao, Energy and exergy analysis of different Trombe walls, Energy and Buildings http://dx.doi.org/10.1016/j.enbuild.2016.04.052

Energy and exergy analysis of different Trombe walls

Shuangping Duan[a,b], Chengjun Jing[b*] chengjunjing@126.com, Zhiqiang Zhao[a]

[a]Department of Civil Engineering and Architecture, Southwest University of Science and Technology, Mianyang, China

[b]Department of Architecture and Environment, Sichuan University, Chengdu, China

Tel: +8618980892979

[*]Corresponding author.

Highlights

- The thermal performance of two types of Trombe walls was compared.
- The energy efficiency was not high and the exergy efficiency was very low.
- The influence factors of energy and exergy efficiencies were obtained.
- The exergy destruction due to absorption of the absorber plate was the largest.
- Two effective methods to increase energy and exergy efficiencies were obtained.

Abstract

This study aims to compare the thermal performance of two different types of Trombe wall: one with the absorber plate pasted on the thermal storage wall (Type I) and one with the absorber plate placed between the glass cover and the thermal storage wall(Type II). The glass cover is double glazed. The energy and exergy efficiencies of the Trombe walls are evaluated for various air channel depths and solar radiation intensities. Based on the energy and exergy efficiencies, the Trombe wall with the absorber plate placed between the glass cover and the thermal storage wall(Type II) is more effective, and the airflow rate and air temperature rise in the air channel is higher than in the Trombe wall with the absorber plate pasted on the thermal storage wall(Type I). In addition, it is found that the particular exergy destruction due to absorption of the absorber plate is the largest and that a higher absorber plate temperature is preferable in decreasing the total exergy destruction and the increasing exergy efficiency.

Keywords: Trombe wall; energy efficiency; exergy efficiency; solar radiation

Introduction

One of the classical passive solar systems is the Trombe wall. A Trombe wall, which is also known as a thermal storage wall and solar heating wall [1,2], reduces a building's energy consumption by up to 30% [3] and provides thermal comfort in winter and intermediate seasons[4]. A Trombe wall is an important green architectural feature that aides the ventilation, heating and cooling of buildings.

Many theoretical and experimental studies on the performance of Trombe walls have been carried out. Khedari et al. investigated the performance of a modified Trombe wall, named the partially-glazed modified Trombe wall, which aimed to induce higher natural ventilation and provide daylight for housing[5]. The thermal performance of two types of solar facade: flat and transpired aluminum plates were compared and it was found that the transpired design was able to reduce heat losses[6]. The thermal performance of a classical Trombe wall and a composite Trombe–Michel wall was also studied[7]. It showed that the composite wall had better energy performance than the classical wall in cold and/or cloudy weather. Ryan et al. reported on test rigs resembling lightweight passive solar air-heating collectors. The thermal efficiency was shown to be a function of the heat input and the system height, but not of the channel depth[8]. The thermal performance of five different passive solar test-cells (Direct -gain, Trombe-wall, Water-wall, Sunspace, and Roofpond) was reported[9]. A research project was conducted to investigate the performance of a coupled novel triple glass and PCM wall as a solar space heater[10]. The energy performance comparison of single glass, double glass and a semi-transparent PV module integrated on the Trombe wall façade of a model test room built in Izmir, Turkey has been carried out[11]. The efficiency of the modified Trombe wall with forced convection that could be operated in four different modes was analyzed[12]. A PV-Trombe wall, installed in a fenestrated room with heat storage, was investigated to approach the practical application of this type of solar wall[13].

Most of the studies on Trombe walls were based on the energy balance equations. However, the energy balance equations alone don't consider the internal losses, and the energy efficiency is not a adequate criterion for Trombe walls. Exergy analysis can reflect the quality change of solar energy transfer process, use and consumption through Trombe walls . Exergy analysis is more informative with regard to the optimum operating zone, quantifying the inefficiencies, their relative magnitudes and locations [14–16]. Exergy is the maximum work potential that can be obtained from a form of energy [17]. Exergy efficiency is more realistic than energy efficiency, and exergy analysis should be considered in the evaluation and comparison of solar thermal systems[18]. Therefore, the main consideration in this study will be on the detailed energy and exergy analysis of two types of Trombe walls , one has the absorber plate pasted on the thermal storage wall(Type I) and one has the absorber plate placed between the glass cover and the thermal storage wall(Type II), these are for evaluating the performance and optimizing the designed Trombe walls with the maximum exergy efficiency under given operating conditions.

2. The description of Trombe walls

Figure 1 shows the physical model for the two types of Trombe walls, and is divided as follows : the glass cover, the absorber plate, the air channel , the thermal storage wall and two openings. Two openings are respectively located on the upper and lower part of the thermal storage wall. In Fig.1(a) , the absorber plate is pasted on the thermal storage wall(Type I) and there is an air channel exists between the glass cover and the absorber plate. In Fig.1(b), the absorber plate is placed between the glass cover and the thermal storage wall(Type II), so there is a air gap between the glass cover and the absorber plate , with the air channel between the absorber plate and the thermal storage wall. The glass cover is double glazed in Fig.1. Solar radiation penetrates through the glass cover and is absorbed by the absorber plate which results in a temperature rise of the absorber plate. Colder air from indoor enters the air channel through the lower opening, and is then heated by the hot absorber plate and rises and enters the indoor through the upper opening. The heat transfer modes and heat exchange in the system are shown in Figure 1.

3. Energy analysis

The energy balance equations are derived , making the following assumptions:

(1) The systems operate under steady state conditions.

(2) The air temperature in air channel changes only in the direction of the flow.

(3) Heat transfer through the glass cover, the absorber plate, and the thermal storage wall is 1-D and in the direction perpendicular to the air flow.

(4) The heat loss of the lateral walls is neglected due to its small effect.

For the studied Trombe walls shown in Fig.1, the energy balance equations are written as below.

The glass cover is double glazed which has four surfaces and one air layer .The first and second surfaces of the glass cover(T_{g1} and T_{g2}) are:

$$h_{c,g-a}A_g(T_{g1}-T_a)+h_{r,g-s}A_g(T_{g1}-T_a)+\frac{\lambda_g}{\delta_g}A_g(T_{g1}-T_{g2})=\alpha_g A_g I \quad (1)$$

$$(h_{r,g-g}+\frac{\lambda_{f,g-g}}{\delta_{f,g-g}})A_g(T_{g2}-T_{g3})+\frac{\lambda_g}{\delta_g}A_g(T_{g2}-T_{g1})=0 \quad (2)$$

where T_{g1}, T_{g2}, T_{g3} are respectively the temperatures of the first, second and third surfaces of the double glazing shown in Fig.1(℃), T_a is the outdoor temperature(℃), A_g is the area of the double glazing (m^2), I is the solar radiation intensity(W/m^2), α_g is the absorptivity of the glass cover, λ_g , $\lambda_{f,g-g}$ are respectively the heat conduction coefficients of the glass and air in the air layer(W/m·K), δ_g , $\delta_{f,g-g}$ are respectively the thickness of the glass and the air layer(m).

The convection heat transfer coefficient due to wind $h_{c,g-a}$ is given by Duffie and Beckmann as [19]:

$$h_{c,g-a} = 5.7 + 3.8u_w$$

where u_w is the wind speed.

The radiation heat transfer coefficient $h_{c,g-s}$ from the outside surface of the double glazing to the sky referred to the ambient temperature is obtained from

$$h_{r,g-s} = \frac{\sigma_b \varepsilon_{g1}({T_{g1}}^4 - {T_s}^4)}{T_{g1} - T_a}$$

where σ_b is Stefan–Boltzmann constant ($5.67 \times 10^{-8} W/m^2 \cdot K^4$), and ε_{g1} is the emissivity of the first surface of the glass cover.

The sky temperature T_s is given by Swinbank [20] as

$$T_s = 0.0552 T_a^{1.5}$$

The radiation heat transfer coefficient $h_{c,g-g}$ from the third surface to the second surface of the double glazing can be derived as

$$h_{r,g-g} = \frac{\sigma({T_{g3}}^2 + {T_{g2}}^2)(T_{g3} + T_{g2})}{\frac{1}{\varepsilon_{g3}} + \frac{1}{\varepsilon_{g2}} - 1}$$

where ε_{g2}, ε_{g3} are respectively the emissivities of the second and third surfaces of the double glazing.

The third and fourth surfaces of the double glazing (T_{g3} and T_{g4}) are:

$$(h_{r,g-g} + \frac{\lambda_{f,g-g}}{\delta_{f,g-g}})A_g(T_{g3} - T_{g2}) + \frac{\lambda_g}{\delta_g} A_g(T_{g3} - T_{g4}) = \alpha_g A_g \tau_g I \quad (3)$$

$$(h_{r,p-g} + \frac{\lambda_{f,p-g}}{\delta_{f,p-g}})A_p(T_{g4} - T_p) + \frac{\lambda_g}{\delta_g} A_g(T_{g4} - T_{g3}) + h_{c,g-f} A_g(T_{g4} - T_f) = 0 \quad (4)$$

where T_{g4} is the temperature of the fourth surfaces of the double glazing, T_p ,T_f are respectively the temperature of the absorber plate and air in air channel (℃), τ_g is the transmissivity of the double glazing. A_p is the area of the absorber plate(m^2), $\lambda_{f,p-g}$ is the heat conduction coefficient of the glass and air in air layer(W/m·K), $\delta_{f,p-g}$ is the thickness of the glass and the air layer(m).

The radiation heat transfer coefficient $h_{r,p-g}$ from the absorber plate to the fourth surface of the double glazing can be obtained from

$$h_{r,p-g} = \frac{\sigma({T_p}^2 + {T_{g4}}^2)(T_p + T_{g4})}{\frac{1}{\varepsilon_p} + \frac{1}{\varepsilon_{g4}} - 1}$$

where ε_p, ε_{g4} are respectively the emissivities of the fourth surface of the double glazing and the absorber plate.

The convection heat transfer coefficient $h_{c,g-f}$ between the air in the air channel and the fourth surface of the double glazing can be defined as

$$h_{c,g-f} = Nu\lambda_f / \delta$$

where λ_f is the heat conduction coefficient of air in air channel (W/m·K), δ is the thickness of the air channel(m). *Nu* is Nusselt number .

For Fig.1(a), $\lambda_{f,p-g} / \delta_{f,p-g} = 0$ in Eq.(3); For Fig.1(b), $h_{c,g-f} = 0$ in Eq.(4).

For the absorber plate(T_p):

$$h_{c,p-f}A_p(T_p - T_f) + (h_{r,p-g} + \frac{\lambda_{f,p-g}}{\delta_{f,p-g}})A_p(T_p - T_{g4}) + U_pA_p(T_p - T_n) + h_{r,p-w}A_p(T_p - T_w) = \alpha_p\tau_gA_pI \quad (5)$$

where T_w is the temperature of the thermal storage wall (℃), T_n is the indoor temperature(℃).

The radiation heat transfer coefficient $h_{r,p-w}$ from the absorber plate to the thermal storage wall can be obtained from

$$h_{r,p-w} = \frac{\sigma({T_p}^2 + {T_w}^2)(T_p + T_w)}{\frac{1}{\varepsilon_p} + \frac{1}{\varepsilon_w} - 1}$$

where ε_w is the emissivity of the outside surface of the thermal storage wall.

The heat transfer coefficient U_p through the thermal storage wall is given as

$$U_p = \frac{1}{\frac{\delta_w}{\lambda_w} + \frac{\delta_{in}}{\lambda_{in}} + \frac{1}{h_n}}$$

where λ_w, λ_{in} are the heat conduction coefficient of the thermal storage material and thermal insulation material (W/m·K), $\delta_{f,p-g}$ is the thickness of the thermal storage and insulation layers(m), h_n is the convection heat transfer coefficient between the thermal storage wall and indoor air(W/m^2·K).

The convection heat transfer coefficient $h_{c,p-f}$ between the air in air channel and the absorber plate may be defined as

$$h_{c,p-f} = Nu\lambda_f / \delta$$

Fig.1(a) , $\lambda_{f,p-g} / \delta_{f,p-g} = 0$, $h_{r,p-w} = 0$ in Eq.(5) ; For Fig.1(b), $U_p = 0$ in Eq.(5).

For the air in the air channel(T_f) :

$$h_{c,p-f}A_p(T_p-T_f)+h_{c,g-f}A_g(T_{g4}-T_f)+h_{c,w-f}A_w(T_w-T_f)=\rho_f qc_p(T_{out}-T_n) \quad (6)$$

where ρ_f is the air density(kg/m^3), q is the airflow rate (m^3/s), c_p is the specific heat of air(J/kg·K), T_{out} is the outlet air temperature (℃).

The convection heat transfer coefficient $h_{c,w-f}$ between the air in air channel and the thermal storage wall in Fig.2 can be defined as

$$h_{c,w-f}=Nu\lambda_f/\delta$$

For Fig.1(a), $h_{c,w-f}=0$ in Eq.(6); For Fig.1(b), $h_{c,g-f}=0$ in Eq.(6).

The mean air temperature in air channel is calculated from[21]

$$T_f=\gamma T_{out}+(1-\gamma)T_n$$

where $\gamma=0.74$

For Fig.1(b), the outside surface of thermal storage wall(T_w):

$$h_{c,w-f}A_w(T_w-T_f)+U_pA_b(T_w-T_n)+h_{r,p-w}A_p(T_w-T_p)=0 \quad (7)$$

where A_w is the area of the thermal storage wall(m^2).

The airflow rate q can be derived as

$$q=c_dA^*\sqrt{2gH\frac{|T_{out}-T_n|}{T_n}} \quad (8)$$

where c_d is the discharge coefficient, c_d=0.57[22], A^* is the effective area of the openings(m^2), $A^*=\sqrt{2}A_tA_b/\sqrt{A_b^2+A_t^2}$, A_t and A_b are respectively the areas of the upper opening and the lower opening(m^2), H is the vertical distance of two openings(m).

The Nusselt number for laminar ($6000<Ra\le 2\times10^5$) and turbulent ($2\times10^5<Ra<1.1\times10^7$) natural convection flow is calculated by using the Eqs.(9) and (10), respectively [23].

$$Nu=0.197Ra^{\frac{1}{4}}(\delta/H)^{\frac{1}{9}} \quad (9)$$

$$Nu=0.073Ra^{\frac{1}{3}}(\delta/H)^{\frac{1}{9}} \quad (10)$$

where $Ra=Gr\,\mathrm{Pr}$, $Gr=g\beta\delta^3\Delta T/\nu_f^2$, $\mathrm{Pr}=\lambda_f/\rho_fc_p\nu_f$, β is the coefficient of thermal expansion(K^{-1}), ΔT is the temperature difference of surfaces(℃).

The density, thermal conductivity, and kinematic viscosity coefficient of air can be obtained from the

equations below[24].

$$\rho_f = 1.1614 - 0.00353(T_f - 300)$$

$$\lambda_f = 0.0263 + 0.000074(T_f - 300)$$

$$\nu_f = [1.846 + 0.00472(T_f - 300)] \times 10^{-5} / \rho_f$$

$$c_p = 1007 + 0.04(T_f - 300)$$

The total heat supply from Trombe walls is given below.

For Fig.1(a):

$$Q_z = \rho_f q c_p (T_f - T_n)/\gamma + U_p A_p (T_p - T_n) \quad (11)$$

For Fig.1(b):

$$Q_z = \rho_f q c_p (T_f - T_n)/\gamma + U_p A_w (T_w - T_n) \quad (12)$$

The energy efficiency of Trombe wall is defined as

$$\eta_1 = \frac{Q_z}{IA_p} \quad (13)$$

4. Exergy analysis

The exergy balance equation for a Trombe wall can be written as:

$$Ex_{sun} + Ex_{mass,in} - Ex_{mas,out} = Ex_{dest} \quad (14)$$

where Ex_{sun} is the solar exergy(W), $Ex_{mass,in}$ is the inlet exergy(W), $Ex_{mass,out}$ is the outlet exergy (W), Ex_{dest} is the exergy destruction(W).

Solar exergy Ex_{sun} can be introduced as[25]:

$$Ex_{sun} = IA_g(1 - \frac{T_a}{T_{sun}}) \quad (15)$$

Considering that the effective sun temperature T_{sun} is 3/4 sun temperature as black body, T_{sun} = 4500 K [26].

Useful exergy Ex_{useful} is the amount of increase in exergy level of the air leaving the lower opening.

$$Ex_{useful} = Ex_{mass,out} - Ex_{mass,in} = \rho_f q[c_p(T_{out} - T_n) - T_a(c_v Ln\frac{T_{out}}{T_n} - R\ln\frac{\rho_{out}}{\rho_n})] \quad (16)$$

where ρ_n is the inlet air density (kg/m^3), ρ_{out} is the outlet air density (kg/m^3), c_v is the constant-volume

specific heat of air(J/kg·K) , R is the gas constant (J/kg·K).

Eq.(16) gives the kinetic energy (exergy) transferred by free convection to the air channel. The amount of exergy gets transferred into the kinetic energy of the air flow, thereby offsetting high-quality electricity (pure exergy) that would power fans.

On the other hand, the exergy destruction may be divided into the following parts.

For Fig.1(a),

$$Ex_{dest} = Ex_{dest,1} + Ex_{dest,2} + Ex_{dest,3} + Ex_{dest,4} + Ex_{dest,5a} + Ex_{dest,6a} + Ex_{dest,7a}$$

For Fig.1(b),

$$Ex_{dest} = Ex_{dest,1} + Ex_{dest,2} + Ex_{dest,3} + Ex_{dest,4} + Ex_{dest,5b} + Ex_{dest,6b} + Ex_{dest,7b} + Ex_{dest,8}$$

Ignoring the exergy destruction due to fluid friction, exergy destruction from the double glazing are due to glass emission and heat convection, so

$$Ex_{dest,1} = \varepsilon_{g1}\sigma_b A_g ({T_{g1}}^4 - {T_a}^4)(1-\frac{T_a}{T_{g1}}) + h_{c,g-a}A_g(T_{g1}-T_a)(1-\frac{T_a}{T_{g1}}) \quad (17)$$

On the right hand side of Eq.(17), the first term is the exergy destruction due to glass emission, and the second term is the exergy destruction due to heat convection.

Exergy destruction due to absorption of the glass cover:

$$Ex_{dest,2} = IA_g\alpha_g(\frac{T_a}{T_{g1}} - \frac{T_a}{T_{sun}}) + IA_g\tau_g\alpha_g(\frac{T_a}{T_{g3}} - \frac{T_a}{T_{sun}}) \quad (18)$$

In the right hand in Eq.(18), the first term is exergy destruction due to absorption of the first layer glass, the second term is exergy destruction due to absorption of the second layer glass.

Exergy destruction due to radiation and heat conduction of the double glazing is:

$$\begin{aligned} Ex_{dest,3} &= \frac{\lambda_g}{\delta_g}A_g(T_{g2}-T_{g1})(\frac{T_a}{T_{g1}} - \frac{T_a}{T_{g2}}) + \frac{\lambda_g}{\delta_g}A_g(T_{g4}-T_{g3})(\frac{T_a}{T_{g3}} - \frac{T_a}{T_{g4}}) \\ &+ \frac{\lambda_{f,g-g}}{\delta_{f,g-g}}A_g(T_{g3}-T_{g2})(\frac{T_a}{T_{g2}} - \frac{T_a}{T_{g3}}) + \frac{\sigma_b A_g({T_{g3}}^4 - {T_{g2}}^4)}{1/\varepsilon_{g2} + 1/\varepsilon_{g3} - 1}(\frac{T_a}{T_{g2}} - \frac{T_a}{T_{g3}}) \end{aligned} \quad (19)$$

In the right hand side of Eq.(19), the first ,second and third terms are respectively exergy destruction due to heat conduction of the first layer, second layer glass and air gap, the fourth term is the exergy destruction due to radiation between the second and third surfaces of the double glazing.

Exergy destruction due to absorption of the absorber plate is:

$$Ex_{dest,4} = IA_p\tau_g\alpha_p(\frac{T_a}{T_p} - \frac{T_a}{T_{sun}}) \quad (20)$$

For Fig.1(a), exergy destruction due to convection between the air in channel and the fourth surface of the

double glazing, the absorber plate:

$$Ex_{dest,5a} = T_a[\rho_f qc_p Ln\frac{T_{out}}{T_n} - \frac{Q_1}{T_{g4}} - \frac{Q_2}{T_p}] \quad (21)$$

where $Q_1 + Q_2 = \rho_f qc_p(T_{out} - T_n)$, $Q_1 = h_{c,g-f}A_g(T_{g4} - T_f)$, $Q_2 = h_{c,p-f}A_p(T_p - T_f)$

For Fig.1(b), exergy destruction due to convection between the air in channel and the absorber plate, the external surface of the thermal storage wall is:

$$Ex_{dest,5b} = T_a[\rho_f qc_p Ln\frac{T_{out}}{T_n} - \frac{Q_1}{T_w} - \frac{Q_2}{T_p}] \quad (22)$$

where $Q_1 = h_{c,g-f}A_g(T_w - T_f)$, $Q_2 = h_{c,p-f}A_p(T_p - T_f)$

For Fig.1(a),exergy destruction due to radiation between the absorber plate and the fourth surface of the double glazing is:

$$Ex_{dest,6a} = \frac{\sigma_b A_p({T_p}^4 - {T_{g4}}^4)}{\frac{1}{\varepsilon_p} + \frac{1}{\varepsilon_{g4}} - 1}(\frac{T_a}{T_{g4}} - \frac{T_a}{T_p}) \quad (23)$$

For Fig.1(b),exergy destruction due to radiation and conduction between the absorber plate and the fourth surface of the double glazing is:

$$Ex_{dest,6b} = [\varepsilon_p\sigma_b A_p({T_p}^4 - {T_{g4}}^4) + \frac{\lambda_{f,p-g}}{\delta_{f,p-g}}A_p(T_p - T_{g4})](\frac{T_a}{T_{g4}} - \frac{T_a}{T_p}) \quad (24)$$

For Fig.1(a),exergy destruction due to heat transfer between the absorber plate and indoor air is:

$$Ex_{dest,7a} = U_p A_p(T_p - T_n)(\frac{T_a}{T_n} - \frac{T_a}{T_p}) \quad (25)$$

For Fig.1(b),exergy destruction due to heat transfer between the external surface of the thermal storage wall and indoor air is:

$$Ex_{dest,7b} = U_p A_p(T_w - T_n)(\frac{T_a}{T_n} - \frac{T_a}{T_w}) \quad (26)$$

For Fig.1(b),exergy destruction due to radiation between the absorber plate and the outside surface of the thermal storage wall is:

$$Ex_{dest,8} = \varepsilon_p\sigma_b A_p({T_p}^4 - {T_w}^4)(\frac{T_a}{T_w} - \frac{T_a}{T_p}) \quad (27)$$

Finally, the exergy efficiency is given as

$$\eta_2 = \frac{Ex_{useful}}{Ex_{sun}} = \frac{\rho_f q c_p (T_{out} - T_n - T_a Ln \frac{T_{out}}{T_n})}{IA_g (1 - \frac{T_a}{T_{sun}})} \quad (28)$$

5.Results and discussion

As a numerical example, it is assumed that T_a = 278 K, T_n=287K. The glass cover is 3m height and 3m wide, which has two layer glass 0.006m(λ_g=0.65W/m·K) and one layer air 0.012m in thickness. The dimensions of the upper and lower openings are 0.2m × 2.0m. The thicknesses of the air channel are 0.1m, 0.2m and 0.3m. The transmissivity and absorptivity of glass are respectively 0.85 and 0.05. The absorptivity and emissivity of the absorber plate are respectively 0.95 and 0.85. The thermal storage wall includes 0.2m of reinforced concrete (λ_w=1.547W/m·K)and a 0.08m insulation layer(λ_{in}=0.047W/m·K).

The five temperatures(T_{g1},T_{g2},T_{g3},T_{g4},T_p,T_f,T_w) and airflow rate in Eqs. (1)~(8) are solved by an iteration method, and the iteration process continues until the convergence value is 10^{-6}. The energy efficiency, solar exergy, useful exergy, exergy destruction and exergy efficiency are solved by substituting the obtained temperatures into Eqs. (13)~(28). The results are shown in Fig.2~6. Numerical results are presented for the effects of different parameters on the thermal performance of Trombe walls with natural convection flow. The parameters include air channel depth, solar radiation intensity, emissivity of the glass cover.

5.1 The effect of solar radiation intensity

Fig.2 and Fig.3 show the variation of energy efficiency and exergy efficiency with solar radiation intensity for the two types of Trombe walls. From Fig.2 and Fig.3, for the first type of Trombe wall (Type I), with the increase of solar radiation intensity up to a certain point, the energy and exergy efficiencies increase and reach maximum values. With further increase in solar radiation intensity, the energy efficiency decreases. The highest energy efficiency is found at solar radiation intensity of around 600W/m^2. However, the exergy efficiency reaches its maximum value when the solar radiation intensity increases to a value larger than 1000W/m^2, which is not shown in Fig.2.

For the second type of Trombe wall(Type II), the energy efficiency decreases with solar radiation intensity and a negative relationship between energy efficiency and solar radiation intensity was observed, as shown in Fig.2. From Fig.3, with the increase of solar radiation intensity up to a certain point, the exergy efficiency increases and reaches its maximum value and then decreases with further increase in solar radiation intensity. It is found that the highest exergy efficiency exists at a solar radiation intensity of around 900W/m^2.

5.2 The effect of air channel depth

From Fig.2 and Fig.3, both the energy efficiency and exergy efficiency increase with air channel depth for the two types of Trombe walls for the given solar radiation intensity. With the increase of air channel depth, the cross-sectional flow area of the air channel increases, and buoyancy forces overcome the friction forces and cause the mass flow rate to increase in the air channel. Hence, the air velocity and consequently heat transfer coefficient will increase. With an increase in the heat transfer coefficient, the heat transfer rate to the air flow, and consequently the energy efficiency and the outlet temperature of air flow will increase. Variation of the exergy efficiency is dependent on the reciprocal effects of the energy efficiency and outlet air temperature. So the exergy efficiency increases with the channel depth.

5.3 Comparison between two types of Trombe walls

From Fig.2 and Fig.3, it is also found that the energy and exergy efficiencies of the second type of Trombe wall (Type II) are higher than that of the first type of Trombe wall(Type I) at the same solar radiation intensity and air channel depth, which are also shown in table 1. In addition, Fig.4 shows variation of the airflow rate and the air temperature rise in the air channel with solar radiation intensity for the two types of Trombe walls when $\delta = 0.1m$ and the emissivities of the four surfaces of the double glazing are 0.84. From Fig.4, the airflow rate and air temperature rise increase with solar radiation intensity. At the same solar radiation intensity, both the airflow rate and air temperature rise in the second type of Trombe wall (Type II) exceed those in the first type of Trombe wall(Type I).

5.4 The effect of emissivity of the glass cover

The emissivities of the four surfaces of the double glazing are 0.84 in Fig.2 and Fig.3. Fig.5 and Fig.6 shows variation of energy and exergy efficiencies with solar intensity and emissivities when $\delta = 0.1m$ for the first type of Trombe wall(Type I). As examples, we change the emissivities of the fourth surfaces of the double glazing. With a decrease in emissivity, the energy and exergy efficiencies increase greatly. Moreover, the emissivity of the fourth surface of the double glazing has a more important effect on the energy and exergy efficiencies than that of other surfaces of the double glazing. So a decrease in emissivity of the fourth surface is an effective method to increase the energy and exergy efficiencies.

5.5 Exergy destruction

Although the energy efficiency is relatively high for two types of Trombe walls, the exergy efficiency is very low. This is because the exergy destruction is too high in the exergy transfer. From table 1, the exergy destruction due to absorption of the absorber plate is the largest among all types of exergy destruction. In the exergy destruction due to absorption of the glass cover and convection between the air in the air channel and the glass cover, between the air in the air channel and the absorber plate also holds the greater proportion. Other forms of exergy destruction are lower. Hence, a decrease in exergy destruction due to

absorption of the absorber plate is an effective method to increase the exergy efficiency. From Eq.(22), an increase in the temperature of the absorber plate can decrease the exergy destruction due to absorption of the absorber plate and hence increase the exergy efficiency.

6.Conclusions

Two types of Trombe walls with natural convection flow have been studied in this research work, and the effects of different parameters from the viewpoints of the first and second laws of thermodynamics have been investigated. The energy efficiency, exergy efficiency and exergy destruction are analyzed. It is concluded that in the second type of Trombe wall(Type II), the temperature of the absorber plate and thus the heat transfer to the air flow is greater than in the collector with the first type of Trombe wall(Type I); therefore, their energy and exergy efficiencies are greater. The increase of parameters such as air channel depth and solar radiation intensity up to a definite point has a favorable effect on the performance of the systems. The decrease of emissivity of the glass cover, especially the fourth surface of the double glazing, is an effective method to decrease exergy destruction and increase energy and exergy efficiencies. Among all the exergy destruction, that due to absorption of the absorber plate is the largest. The another effective method to decrease the total exergy destruction and increase the energy and exergy efficiencies is to increase the temperature of the absorber plate.

Acknowledgements

The authors gratefully acknowledge the funding by the Natural Scientific Foundation of China(51208442).

References

[1] Hami K, Draoui B, Hami O , The thermal performances of a solar wall. Energy 39 (2012) 11-16.

[2] Fang X, Yang T. Regression methodology for sensitivity analysis of solar heating walls. Applied Thermal Engineering 28 (2008) 2289–2294.

[3] Hordeski MF , New technologies for energy efficiency. New York:The Fairmont Press (2011) .

[4] Francesca Stazi, Alessio Mastrucci , Costanzo di Perna , The behavior of solar walls in residential buildings with different insulation levels: An experimental and numerical study. Energy and Buildings 47 (2012) 217–229.

[5] Khedari J., Pongsatirat C., Puangsombut W., Hirunlabh J , Experimental performance of partially-glazed modified Trombe wall. International Journal of Ambient Energy 26 (2005) 27–36.

[6] Hoy Yen Chan, Jie Zhu, Mohd Hafidz Ruslan , Kamaruzzaman Sopian , Saffa Riffat , Thermal analysis of flat and transpired solar facades. Energy Procedia 48 (2014) 1345 – 1354.

[7] Jibao Shen , Ste phane Lassue, Laurent Zalewski , Dezhong Huang , Numerical study on thermal behavior of classical or composite Trombe solar walls. Energy and Buildings 39 (2007) 962–974.

[8] D. Ryan, S.A.M. Burek , Experimental study of the influence of collector height on the steady state performance of a passive solar air heater . Solar Energy 84 (2010) 1676–1684 .

[9] Alfredo Ferna ´ndez-Gonza ´lez , Analysis of the thermal performance and comfort conditions produced by five different passive solar heating strategies in the United States Midwest .Solar Energy 81 (2007) 581–593.

[10] Yusuf Ali Kara , Aslıhan Kurnuc , Performance of coupled novel triple glass and phase change material wall in the heating season: An experimental study, Solar Energy 86 (2012) 2432–2442.

[11] Basak Kundakci Koyunbaba , Zerrin Yilmaz, The comparison of Trombe wall systems with single glass, double glass and PV panels. Renewable Energy 45 (2012) 111-118.

[12] S. Dragicevic, M. Labic , Influence of constructive and operating parameters on a modified Trombe wall efficiency. Archives of Civil and Mechanical Engineering 11 (2011) 825-838.

[13] Jie J., Hua Y., Gang P., Jianping L , Study of PV-Trombe wall installed in a fenestrated room with heat storage, Applied Thermal Engineering 27 (2007) 1507–1515.

[14] Kostic LT, Pavlovic TM, Pavlovic ZT， Influence of reflectance from flat aluminum concentrators on energy efficiency of PV/thermal collector. Applied Energy 87 (2010) 410–416.

[15] Farahat S, Sarhaddi F, Ajam H ,Exergetic optimization of flat plate solar collectors. Renewable Energy 34 (2009) 1169–1174.

[16] Torres-Reyes E, Navarrete-Gonzalez JJ, Cervantes-de Gortari JG，Thermodynamic optimization as an effective tool to design solar heating systems. Energy 29 (2004) 2305–2315.

[17] Bejan A. Advanced engineering thermodynamics，Wiley InterScience Pub（2006）.

[18] Ozturk HH, Demirel Y ,Exergy-based performance analysis of packed-bed solar air heaters. Int J Energy Res 28 (2004) 423–432.

[19] Mcadams W H, Heat Transmission,3rd ed. New York: McGraw-Hill (1994).

[20] Duffie J A, Beckman W A. Solar thermal process. New York: John Wiley & Sons Inc.(1974).

[21] Hirunlabh J, Kongduang W, Namprakai P,et al，Study of natural ventilation of houses by a metallic solar wall under tropical climate. Renewable Energy 18 (1999) 9-19.

[22] Akbarzadeh A., Charters W.W.S., Lesslie D.A. ,Thermo circulation characteristics of a Trombe wall passive test cell, Solar Energy 28 (1982) 461–468.

[23] Min ZX,Ren XP,Mei FM , Heat transmission,3rd ed. Beijing: Architecture Publishing Company of China.（2000）.

[24] Incropera F P, Dewitt D P，Fundamentals of Heat and Mass, 4th ed. New York: John Wiley & Sons Inc.(1996).

[25] Dutta Gupta, K.K., Saha, S, Energy analysis of solar thermal collectors. Renew. Energy Environ. 103 (1990) 283–287.

[26] Bejan, A., Keary, D.W., Kreith, F, Second law analysis and synthesis of solar collector systems. J. Sol. Energy Engineering 103 (1981) 23–28.

Figure Captions

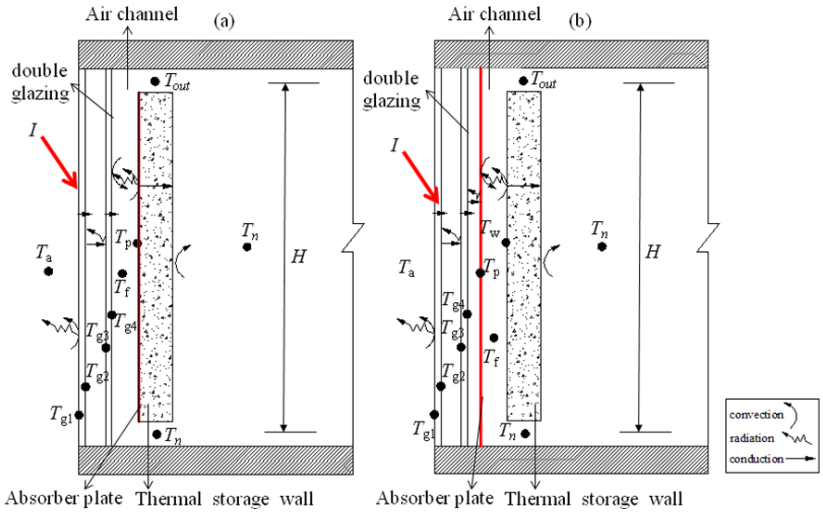

Fig.1 Physical model of Trombe wall. (a) Type I: the absorber plate pasted on the thermal storage wall; (b) Type II: the absorber plate placed between the glass cover and the thermal storage wall

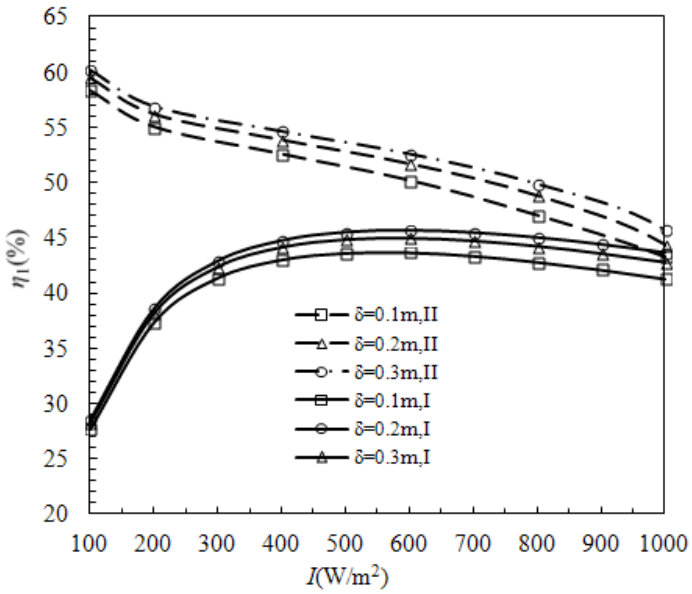

Fig.2 Variation of energy efficiency with channel depth and solar intensity for two types of Trombe walls

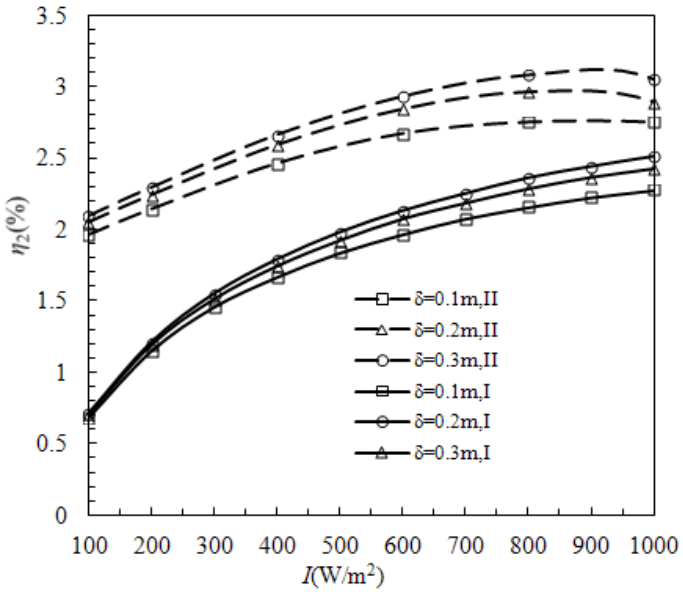

Fig.3 Variation of exergy efficiency with channel depth and solar intensity for two types of Trombe walls

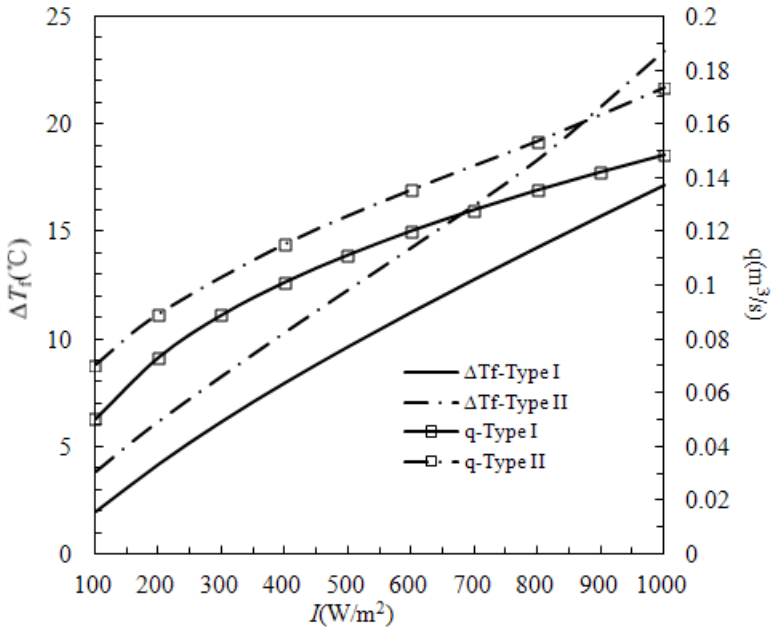

Fig.4 Variation of airflow rate and air temperature rise increase with solar intensity for two types of Trombe walls when $\delta = 0.1m$

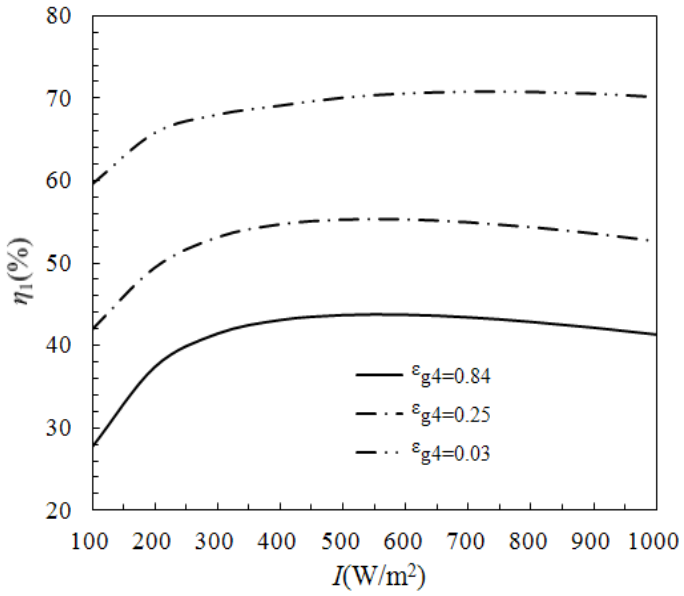

Fig.5 Variation of energy efficiency with **emissivity** for the first type of Trombe wall when $\delta = 0.1m$

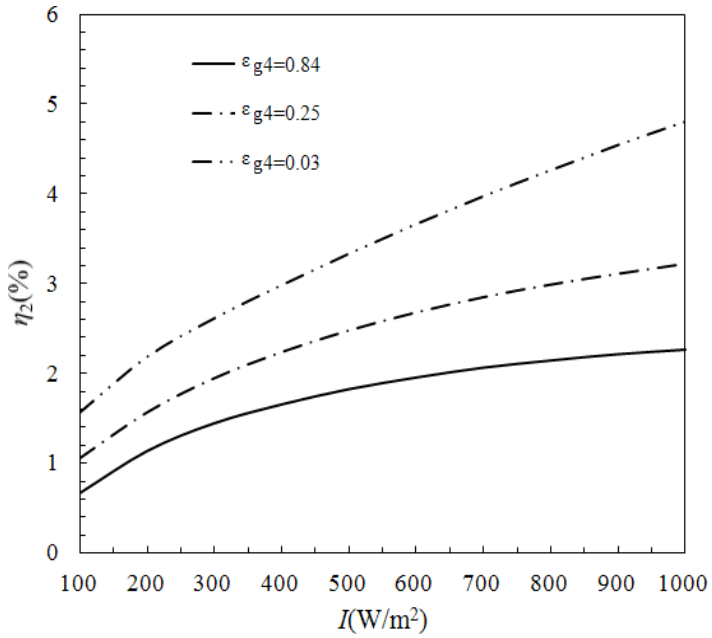

Fig.6 Variation of exergy efficiency with emissivity for the first type of Trombe wall when $\delta = 0.1m$

Table Captions

Table 1 Energy and exergy analysis of Trombe walls($\delta = 0.1m$)

Trombe Wall	I (kW/m^2)	Ex_{solar} (kW)	Ex_{useful} (kW)	$Ex_{dest,1}$ (kW)	$Ex_{dest,2}$ (kW)	$Ex_{dest,3}$ (kW)	$Ex_{dest,4}$ (kW)	$Ex_{dest,5}$ (kW)	$Ex_{dest,6}$ (kW)	$Ex_{dest,7}$ (kW)	η_1(%)	η_2(%)
	0.1	0.844	0.006	0.000	0.142	0.007	0.597	0.006	0.004	0.001	27.69	0.67
Type I	0.2	1.689	0.019	0.007	0.278	0.012	1.127	0.034	0.016	0.002	37.36	1.14
	0.4	3.378	0.056	0.056	0.530	0.019	2.045	0.148	0.057	0.004	43.01	1.66
	0.6	5.066	0.099	0.148	0.760	0.025	2.831	0.308	0.110	0.005	43.65	1.96
	0.8	6.755	0.145	0.290	0.970	0.031	3.518	0.492	0.169	0.006	42.79	2.15
	1	8.444	0.192	0.487	1.161	0.038	4.129	0.683	0.233	0.007	41.27	2.27
	0.1	0.844	0.017	0.004	0.076	0.012	0.669	0.029	0.007	0.002	58.28	1.96
Type II	0.2	1.689	0.036	0.024	0.146	0.017	1.255	0.089	0.020	0.003	55.01	2.14
	0.4	3.378	0.083	0.090	0.275	0.026	2.246	0.275	0.063	0.005	52.55	2.46
	0.6	5.066	0.135	0.210	0.386	0.036	3.040	0.515	0.134	0.006	50.18	2.67
	0.8	6.755	0.186	0.422	0.480	0.046	3.654	0.768	0.242	0.007	47.02	2.75
	1	8.444	0.232	0.794	0.556	0.056	4.100	0.984	0.394	0.009	43.26	2.75